Journal of Marine Research, 59, 675–696, 2001

Journal of
MARINE RESEARCH

Volume 59, Number 5

Mechanism of offshore nutrient supply in the western Arabian Sea

by Michio Kawamiya[1]

ABSTRACT

The mechanism to maintain the high surface chlorophyll in the western Arabian Sea during the southwest monsoon (SWM) season is studied with an eddy-permitting, biological-physical coupled model. Using a set of artificial tracers, it is revealed that horizontal transport of nutrient subsequent to the coastal upwelling is by far more important than the open ocean upwelling due to the Ekman pumping. The horizontal transport can be classified into three processes, the Ekman transport, transport by the large-scale circulation and that by the mesoscale currents. In the model, the first has only a minor effect within the area of high chlorophyll while the latter two have comparable contributions. Considering the fact that simulated eddy activity is still less than observed by satellites, it may be possible to make the model results more realistic by assimilating sea-surface height data or running a finer resolution model.

1. Introduction

In the western Arabian Sea, the southwestern monsoon (SWM) in boreal summer excites a phytoplankton bloom extending from the coasts to the southeast, with a width of ~100 km (Madhupratap and Parulekar, 1993). While it is rather obvious that along-the-coast nutrients are supplied through the coastal upwelling, it has been a matter of argument which process is responsible for the zonal extension of the high chlorophyll band. The main possibilities include horizontal nutrient advection subsequent to the upwelling along the coasts of Oman and Somalia, and vertical nutrient advection due to open-ocean Ekman upwelling.

1. Institut für Meereskunde an der Universität Kiel, Düsternbrooker Weg 20, D-24105, Kiel, Germany. ***email: mkawamiya@ifm.uni-kiel.de***

Banse (1987) put an emphasis on the horizontal advection stating that surface water in the central Arabian Sea (~10N, 65E) seems to have its origin off the coast of Oman. Young and Kindle (1994), using a reduced gravity model with thermodynamics, made experiments in which a tracer that mimics silicate was released. They pointed out that the coastal upwelling and the subsequent horizontal advection is important for the silicate supply off the coast of Oman, though the area they focused upon was much closer to the coast than in the case of Banse (1987). Keen *et al.* (1997) embedded an ecosystem model in the same physical model and obtained a similar result that the horizontal advection is important for nitrate as well. They also showed that the simulated chlorophyll distribution is indeed a reflection of the nitrate field formed through the effect of horizontal advection. In an observational study, Morrison *et al.* (1998) speculated that it is unlikely that the open ocean upwelling dominates nutrient supply to the offshore regions, mentioning that there is some evidence that the open ocean upwelling is often distorted by instability.

Rixen *et al.* (1996) suggested, however, that the open ocean upwelling is as important as the coastal upwelling, analyzing a long time series of particle flux with the help of satellite data. Also, Bartolacci and Luther (1999) found a trace of the effect of the open ocean upwelling in their extensive analyses using statistical methods to relate chlorophyll fields and physical fields such as wind stress.

The conclusions in the above studies have been obtained through similarity in T-S diagram (Banse, 1987), a simple pattern matching (Young and Kindle, 1994; Keen *et al.,* 1997) or a statistical correlation (Rixen *et al.,* 1996; Bartolacci and Luther, 1999). In this study we present, from a numerical modeling point of view, a method to distinguish more directly nutrient lifted up by the coastal upwelling and that by the open ocean upwelling. Furthermore, the horizontal advection of nutrient is divided into three processes, that is, transport by the Ekman flow, mesoscale currents and large-scale circulation. This analysis is motivated because some recent studies (e.g., Manghnani *et al.,* 1998; Flagg and Kim, 1998; Dickey *et al.,* 1998; Fischer *et al.,* 2001) stress the role of mesoscale features in both physical and biological aspects, though a typical traditional view of the horizontal transport in this region of the Arabian Sea is that the Ekman flow is the main carrier as illustrated in Figure 1 of Bartolacci and Luther (1999). Thus, the purpose of this paper is to assess the relative importance of the open ocean upwelling and the coastal upwelling for the formation of the high-chlorophyll band, and to identify the process(es) responsible for horizontal nutrient transport after the vertical transport by the coastal upwelling.

2. Model

Here we describe briefly the model configuration. For further details the readers are referred to Kawamiya and Oschlies (2001) and, for the biological model, Oschlies and Garçon (1999).

a. Physical model

For the physical part of the model, we adopt Modular Ocean Model version 2.1 by Geophysical Fluid Dynamics Laboratory (Pacanowski, 1995), set up for the Indian Ocean by Rix (1998). The model domain extends from 30S to 26N and from 30E to 110E with a realistic bottom topography. The meridional and zonal resolution are both 1/3 degree. There are 35 vertical levels, 10 out of which are within the upper 110 m. The vertical diffusion and viscosity coefficient are calculated with the parameterization by Pacanowski and Philander (1981) with a background diffusion and viscosity coefficient of 0.1 cm^2/s. Horizontal diffusion and viscosity are expressed through a biharmonic operator with a coefficient of 2.5×10^{19} cm^4/s for both.

The model is forced with heat fluxes computed following Haney (1971) using the data sets by Barnier *et al.* (1995). Surface salinity is relaxed to the monthly mean values of Levitus and Boyer (1994a). Wind stress has been taken from the analysis by Barnier *et al.* (1995) on European Centre for Medium-Range Weather Forecasts (ECMWF) data for the years 1986–1988. The open boundary conditions of Stephens (1991) are used for the southern and eastern open boundary. Restoration is necessary when the flow across the open boundaries is inward from outside the domain: for salinity and temperature, monthly mean data by Levitus and Boyer (1994a,b) are used, respectively; for nitrate, needed for the biological model, annual mean data by Conkright *et al.* (1994a) are used.

b. Biological model

The biological model used is a nitrogen-based, four-compartment one whose structure is depicted in Figure 1, where N denotes nitrate, P phytoplankton, Z zooplankton and D detritus. The model variables evolve with time according to a set of the advection-diffusion equations with source-minus-sink (sms) terms representing the biological interactions. The sms terms are formulated as below:

$$\mathrm{sms}(P) = \bar{J}(z, t, N)P - G(P)Z - \mu_P P, \tag{1}$$

$$\mathrm{sms}(Z) = \gamma_1 G(P)Z - \gamma_2 Z - \mu_Z Z^2, \tag{2}$$

$$\mathrm{sms}(D) = (1 - \gamma_1)G(P)Z + \mu_P P + \mu_Z Z^2 - \mu_D D - w_s \frac{\partial D}{\partial z}, \tag{3}$$

$$\mathrm{sms}(N) = \mu_D + \gamma_2 Z - \bar{J}(z, t, N)P, \tag{4}$$

where $\bar{J}$ is the daily averaged phytoplankton growth rate as a function of depth z and time t, and G is the grazing function while other symbols are constant parameters. The parameter values and the exact forms of $\bar{J}$ and G are given by Oschlies and Garçon (1999); the only difference is that the grazing coefficient is reduced from 2/d, a value higher than in other literature such as Fasham *et al.* (1990), to 1/d in this study. In the experiments by Oschlies and Garçon (1999), the high grazing rate was adopted to suppress an unrealistically strong spring bloom. This bloom is associated with a large, sudden retreat of the mixed layer in

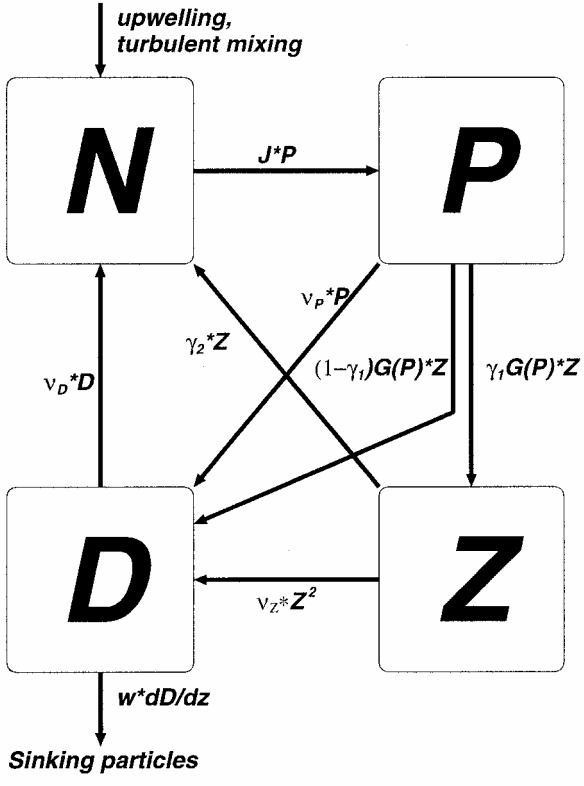

Figure 1. Compartments and interactions of the biological model.

the northern North Atlantic in spring. In the Arabian Sea, annual excursion of the mixed layer is much smaller and more gradual, leaving us no reason to maintain the high grazing pressure in the present model.

c. Model result

The biological-physical coupled model is integrated for 3 years after a stand-alone spin-up of the physical model. The nitrate field has been initialized with the data by Conkright *et al.* (1994b). For the initial concentrations of the other biological variables, values have been set to 0.1 mmol/m^3 everywhere above 500 m depth, and zero below. Results from the third year of the coupled integration will be presented unless otherwise specified.

Kawamiya and Oschlies (2001) extensively compared model results with observations. It was found that the model reproduces the nitrate increase during SWM due to upwelling along the coasts of Oman and Somalia and the consequent phytoplankton bloom. Figure 2 shows surface chlorophyll concentration averaged over the upper 20 m during June–September (corresponding to SWM) obtained by the model and the

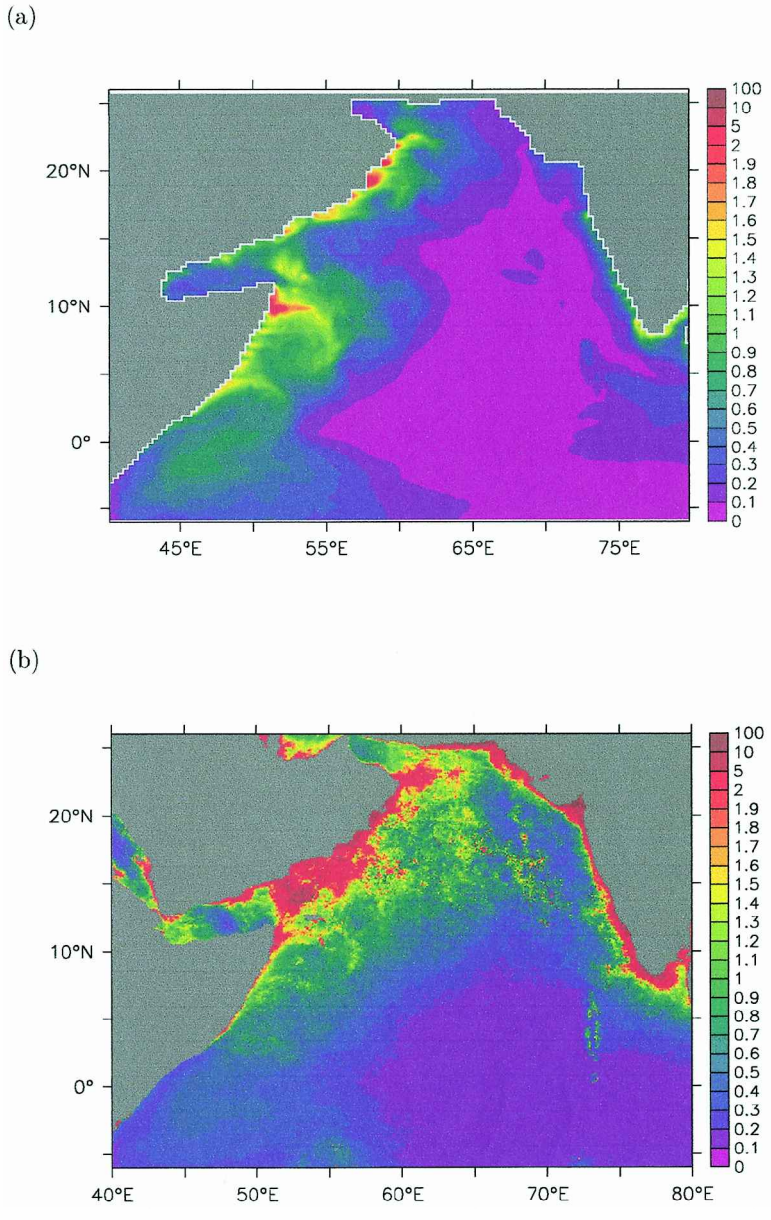

Figure 2. Mean surface chlorophyll distribution over June–September (a) obtained by the model (b) measured by SeaWiFS averaged over the years 1998–2000. Units are μg/l. The model result has been averaged over the upper 20 m. SeaWiFS data are provided by the Earth Observing System Data and Information System (EOSDIS), Distributed Active Archive Center at Goddard Space Flight Center which archives, manages and distributes this dataset through funding from Earth Observing System of NASA's Mission to Planet Earth.

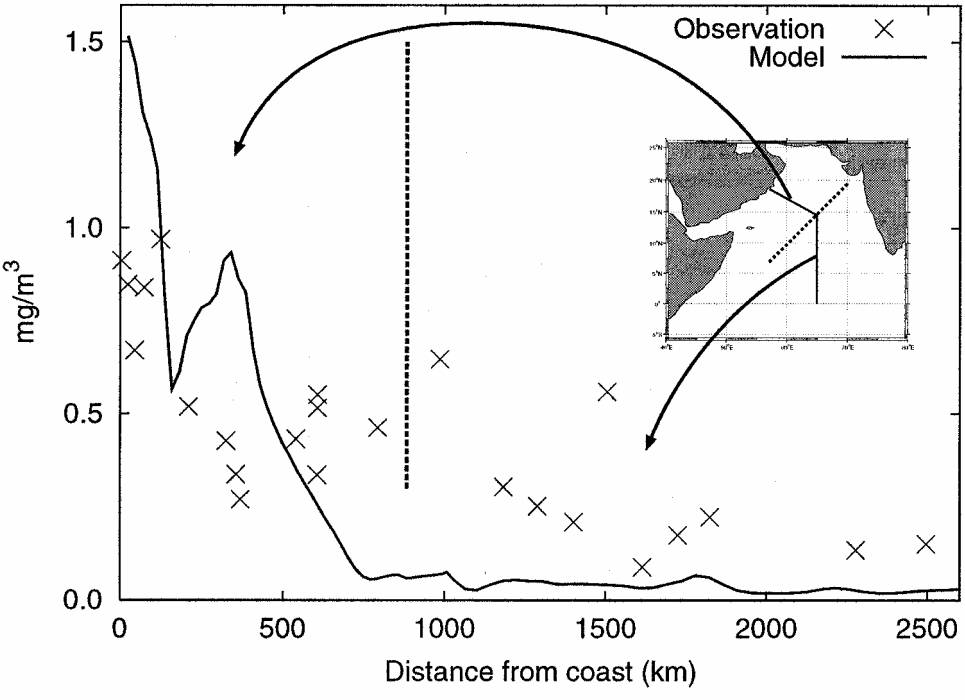

Figure 3. Chlorophyll averaged over the upper 20 m along the line depicted in the inset, which is the observation track by R/V *Meteor* under German JGOFS M32/5 during Jul. 18–Aug. 11, 1995. The horizontal axis is expressed in the distance from the coast measured along the line. The crosses show the values observed during the cruise (data courtesy of Klaus v. Bröckel at IfM Kiel), and the thick line is the model result averaged over the above observation period. The dashed line in the main panel represents the point where the line turns to the south, and corresponds to that in the inset.

satellite observations by SeaWiFS. Chlorophyll values are calculated by using a chlorophyll-to-carbon mass ratio of 1:50 and a C:N mole ratio of 106/16. Both model result and the observations reveal elevated chlorophyll concentration along the coasts of Oman and Somalia with a certain zonal extent, though the concentration is lower and the zonal extent is narrower in the model. While satellite measurements are possibly less reliable in the Arabian Sea during SWM than in other basins due to higher aerosol concentrations and more frequent cloud cover, a similar tendency can be found when the model result is compared with *in situ* data taken during SWM (Fig. 3); the model reproduces the elevated chlorophyll near the coast, though it declines more rapidly than in the data with the distance from the coast. Note, however, that the satellite measurements seem to give too high values very close to the coast. The mechanism creating this spatial extension of chlorophyll enhancement is, as stated in the introductory section, the theme of this study.

3. "Labeled nitrate" experiment

To identify the nutrient source in the offshore regions, we introduce a set of artificial tracers (labeled according to the region where they are upwelled) which are similar to those introduced by Numaguti (1999) in an atmospheric study. They are different from ordinary passive tracers transported only by physical processes in that they can track the fate of nitrate transported through the combination of physical and biological processes. Their governing equations are given below.

a. Formulation

The formulation requires calculation of the ratio of the nitrogen originally upwelled in a certain area to the ambient nitrogen of the compartments of the biological model. In the explanation below it is assumed that there is only one source region for the tracers, in order to avoid complication through the use of too many subscripts. It is straightforward to extend the equations for the case of multiple source regions.

Let r_i and C_i be the above ratio and the concentration of each variable in the biological model, respectively, where $i = 1 \cdots 4$. In the case of $i = 1$, the concentration C_i corresponds to nitrate (N), 2 to phytoplankton (P), 3 to zooplankton (Z) and 4 to detritus (D). The ratio r_i should follow the following equation:

$$\frac{\partial (C_i r_i)}{\partial t} = -\nabla_h (\mathbf{u} C_i r_i) - \frac{\partial \{(w - \delta_{i4} w_s) C_i r_i\}}{\partial z} - K_h \nabla_h^4 (C_i r_i) + \frac{\partial \{\partial (K_v C_i r_i)/\partial z\}}{\partial z} + \sum_{j=1,\, j\neq i}^{4} F_{j\to i} r_j - r_i \sum_{j=1,\, j\neq i}^{4} F_{i\to j} + \text{source}_i, \quad (5)$$

where $\mathbf{u}$ is horizontal velocity vector, w vertical velocity, w_s sinking velocity of detritus, δ_{ij} Kronecker's delta, K_h biharmonic horizontal diffusivity, K_v vertical diffusivity, $F_{j\to i}$ the flux from the compartment j to i computed by the biological model, and source$_i$ the source term given only for the artificial tracer corresponding to nitrate ($C_1 r_1$). The source term is calculated so that vertical advection flux of $C_1 r_1$ across a given depth (z_0) in a source region (denoted as $\mathcal{A}$) is equal to that of nitrate ($wC_1 = wN$) when the vertical velocity is upward; the source term becomes zero whenever the vertical velocity is downward.

$$\text{source}_i = \begin{cases} \max\left[\dfrac{w\{(C_1) - (C_1 r_1)\}\big|_{z=z_0}}{\Delta z_n}, 0 \right] & \text{for } i = 1 \text{ and } k = n \text{ and } \mathbf{x} \in \mathcal{A} \\ 0 & \text{otherwise.} \end{cases} \quad (6)$$

Here, $\mathbf{x}$ denotes latitude and longitude, k is the index for model's discrete vertical level, and n is the level whose bottom lies at the depth z_0. Δz_n is the thickness of the level n. Note that $wC_1 r_1$ should be subtracted in the numerator because this flux is already taken into account in the vertical advection term of the Eq. 5. Figure 4a gives a schematic

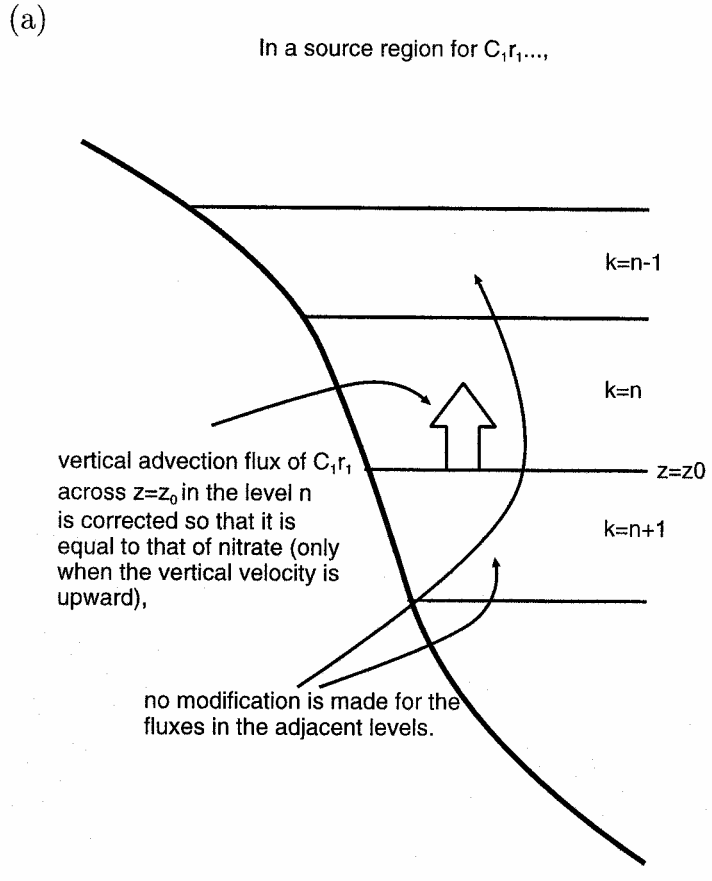

Figure 4. (a) Schematic view of how the source for the tracers is set.

view of how the source term is calculated. Figure 4b shows the distribution of the source regions. They are situated at $z_0 = 110$ m, as a proxy for the bottom of the euphotic zone.

The source regions are set according to upwelling phenomena known to occur during SWM: region 1 corresponds to the coastal and Ekman upwelling region along the coast of Somalia, region 2 to the coastal upwelling along the coast of Oman and region 3 to open ocean Ekman upwelling. The sources are activated from April 1 to October 31 in the third year of integration, covering the SWM season.

b. Result

Figure 5 displays the ratio of the nitrate from each source region to the ambient nitrogen averaged over the period June 1–September 30, and the depth range 0–60 m, namely

(b)

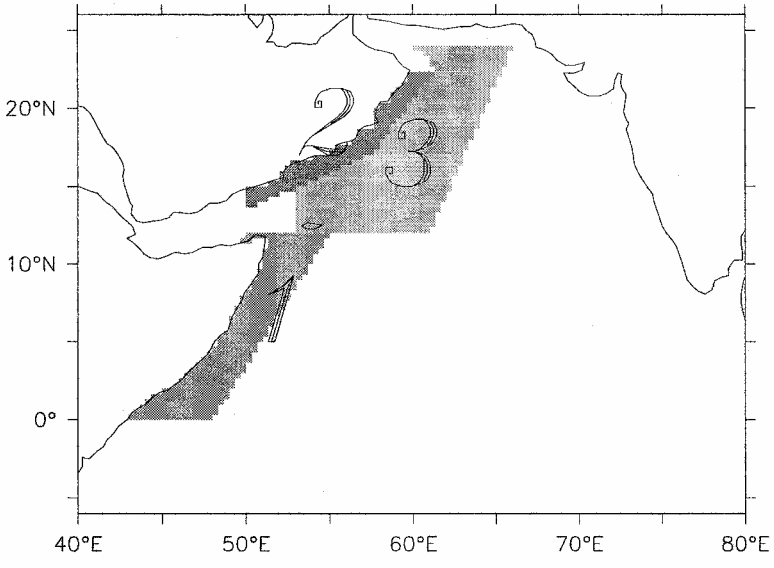

Figure 4. (Continued) (b) Source regions.

$$\frac{\int_{\text{Jun. 1}}^{\text{Sep. 30}} \int_{60\text{ m}}^{0\text{ m}} C_1 r_1 \, dz dt}{\int_{\text{Jun. 1}}^{\text{Sep. 30}} \int_{60\text{ m}}^{0\text{ m}} C_1 \, dz dt}.$$

This depth range is chosen because nitrate below this is often contributing only to form the deep chlorophyll maximum (DCM) and not to increase surface chlorophyll; Kawamiya and Oschlies (2001) showed that the modeled DCM is formed typically at a depth of ~70 m.

It is seen that nitrate from regions 1 and 2 (nitrate upwelled along the coasts of Oman and Somalia) is playing a dominant role in nitrate supply to the offshore regions. Nitrate from region 3 (nitrate upwelled through open ocean Ekman upwelling) is contributing to a much lesser extent; the open ocean upwelling is of a minimal importance. This statement is even reinforced when one considers that the simulated chlorophyll concentration is relatively low during the SWM season in the area where the contribution of nitrate from region 3 is significant (13N–15N, 55E–60E), compared with other areas in the high chlorophyll band (see Fig. 2). Note also that the area is much smaller than that of the source region itself.

In summary, the coastal upwelling and the subsequent horizontal transport are the main

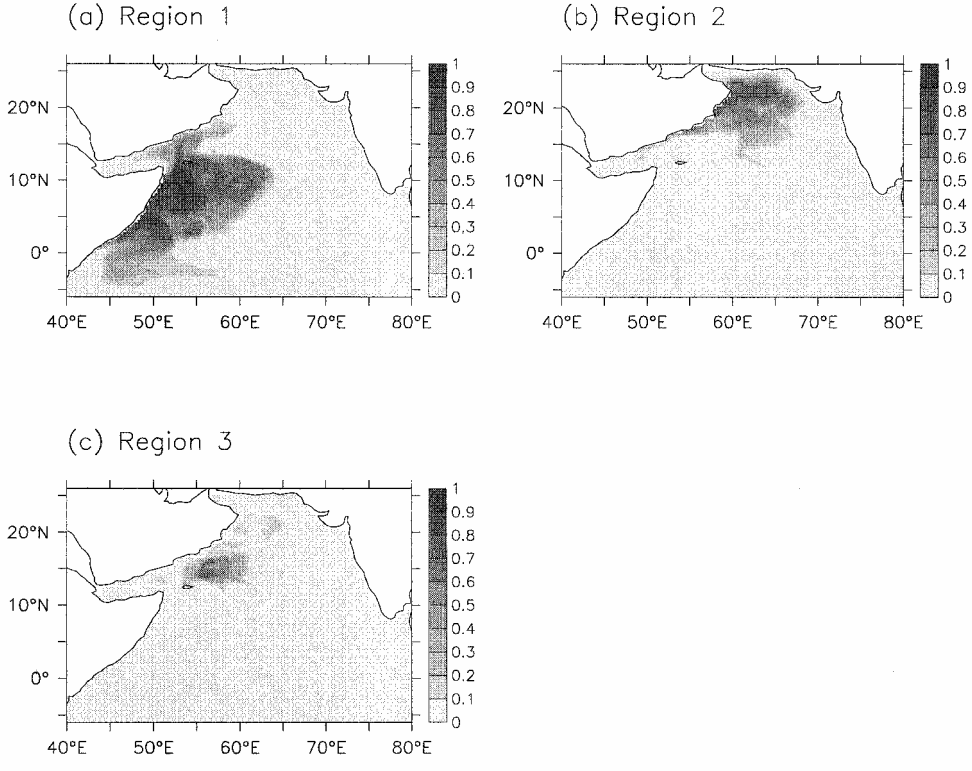

Figure 5. Ratio of the nitrate from each source region displayed in Figure 4b to the ambient nitrogen averaged over the period June 1–September 30 and the depth range 0–60 m.

mechanism to form the zonally extended band of high chlorophyll in the model. To the north of ~15N, the coastal upwelling along the coast of Oman is feeding nitrate to the offshore regions, and to the south, upwelling along the coast of Somalia takes over. It is worth pointing out that the contribution of Somalia upwelling is significant even along the southern fraction of the coast of Oman.

We point out here that strong upwelling can be found along the periphery of the Great Whirl during the SWM season (figures not shown) and could be contributing significantly for the nitrate transport. We did not set a source region for this upwelling because its cause is the dynamics of the Great Whirl and its locations cannot be predicted from the forcing field, unlike in the case of Ekman or the coastal upwelling. Contribution from vertical mixing can be also significant where strong upwelling takes place.

The result that nutrient transport by horizontal advection following the coastal upwelling is the key process is consistent with that of Young and Kindle (1994) and Keen *et al.* (1997). Their conclusion is strengthened by this study where the contribution from each source region is clearly distinguished from one another, as opposed to their study where the

analysis was based on pattern comparison by eyes. Furthermore, they did not point out the importance of the Somalia upwelling.

4. Decomposition of horizontal transport into three processes

A traditional picture on horizontal transport of nutrient off the coasts of Oman and Somalia is that the Ekman transport is the main vehicle for nutrient (e.g., Bartolacci and Luther, 1999). It is, however, still possible that flows due to other processes such as mesoscale currents also provide convenient transportation for nutrients. Here we attempt to decompose horizontal transport of nitrate according to the process, and we estimate the contribution of each process.

a. Definitions

We consider three processes for the decomposition; that is, surface current caused by Ekman dynamics, mesoscale currents which would not be resolved by a typical coarse resolution model nor geostrophic computation from a climatological data set, and large-scale circulation which is analogous to the geostrophic currents based on climatology. The flow field based on each process should be reconstructed from the forcing field or the model result, or both. First, zonal (u_{ek}) and meridional (v_{ek}) Ekman velocity are calculated assuming that the Ekman layer thickness (d) is 30 m,

$$u_{ek}(\mathbf{x}, z, t) = \frac{\sqrt{2}}{\rho_0 f d}\exp(z/d)[\tau^x(\mathbf{x}, t)\cos(z/d - \pi/4) - \tau^y(\mathbf{x}, t)\sin(z/d - \pi/4)],$$

$$v_{ek}(\mathbf{x}, z, t) = \frac{\sqrt{2}}{\rho_0 f d}\exp(z/d)[\tau^x(\mathbf{x}, t)\sin(z/d - \pi/4) + \tau^y(\mathbf{x}, t)\cos(z/d - \pi/4)], \quad (7)$$

where τ^x, τ^y are zonal and meridional wind stress, respectively, ρ_0 the characteristic density of sea water ($\sim$1 g/cm^3) and f the Coriolis parameter (Cushman-Roisin, 1994).

It is not straightforward to distinguish the mesoscale currents and the large-scale circulation. A simple-minded way is to take annual mean to obtain the large-scale circulation, expecting that mesoscale currents are canceled out. In the case of the Arabian Sea, however, even the large-scale circulation will largely cancel out because of the seasonal reversal. On the other hand, if the mean is taken over a much shorter period, for example the SWM season, then mesoscale currents can survive over the whole period and their contribution will be counted as the "large-scale circulation." To obtain the large-scale circulation field, another model run is, therefore, carried out in which the horizontal viscosity is enhanced by expressing it by the Laplacian operator with a coefficient of 10^8 cm^2/s, while retaining biharmonic diffusion (Oschlies and Garçon, 1998). This value is typical of classic coarse resolution models, thereby prohibiting any mesoscale features. This model run will be referred to as the viscous run, while the term standard run will be used for the one from which the results have been shown so far. The integration period for

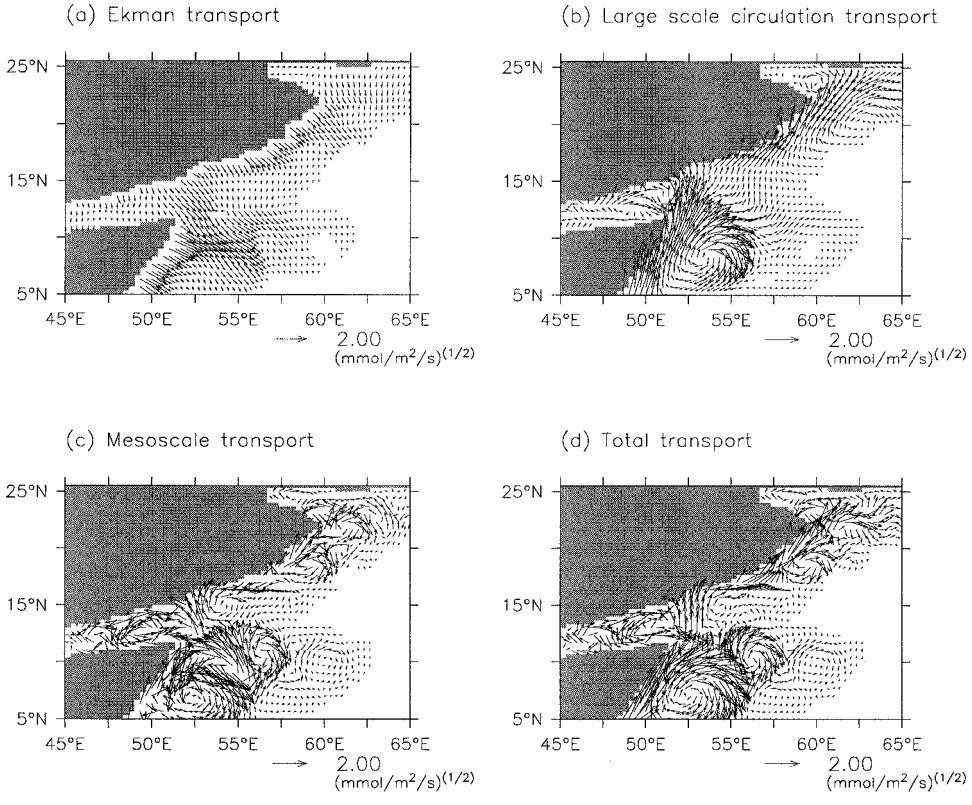

Figure 6. Horizontal advection flux of nitrate averaged over the upper 60 m and June–September, due to (a) Ekman transport, (b) large-scale circulation, (c) mesoscale currents and (d) total current. See text for the definition of the processes. Note that the length of the arrows is proportional to the square root of the absolute value of flux so that arrows with a small value are more visible.

the viscous run is also three years, starting from the same initial conditions as for the standard coupled run. The biological model is embedded as well and a result will be presented later.

The flow field from the third year of the viscous run ($\mathbf{u}_{vis}$) is, after subtracting the Ekman field ($\mathbf{u}_{ek} = (u_{ek}, v_{ek})$), treated as the large-scale circulation ($\mathbf{u}_{lsc}$),

$$\mathbf{u}_{lsc} = \mathbf{u}_{vis} - \mathbf{u}_{ek}. \tag{8}$$

Finally, the flow field due to mesoscale currents ($\mathbf{u}_{msc}$) is defined as the difference between those in the standard and viscous run.

$$\begin{aligned} \mathbf{u}_{msc} &= \mathbf{u}_{tot} - \mathbf{u}_{vis} \\ &= \mathbf{u}_{tot} - \mathbf{u}_{lsc} - \mathbf{u}_{ek}, \end{aligned} \tag{9}$$

where $\mathbf{u}_{tot}$ is total horizontal velocity from the standard run.

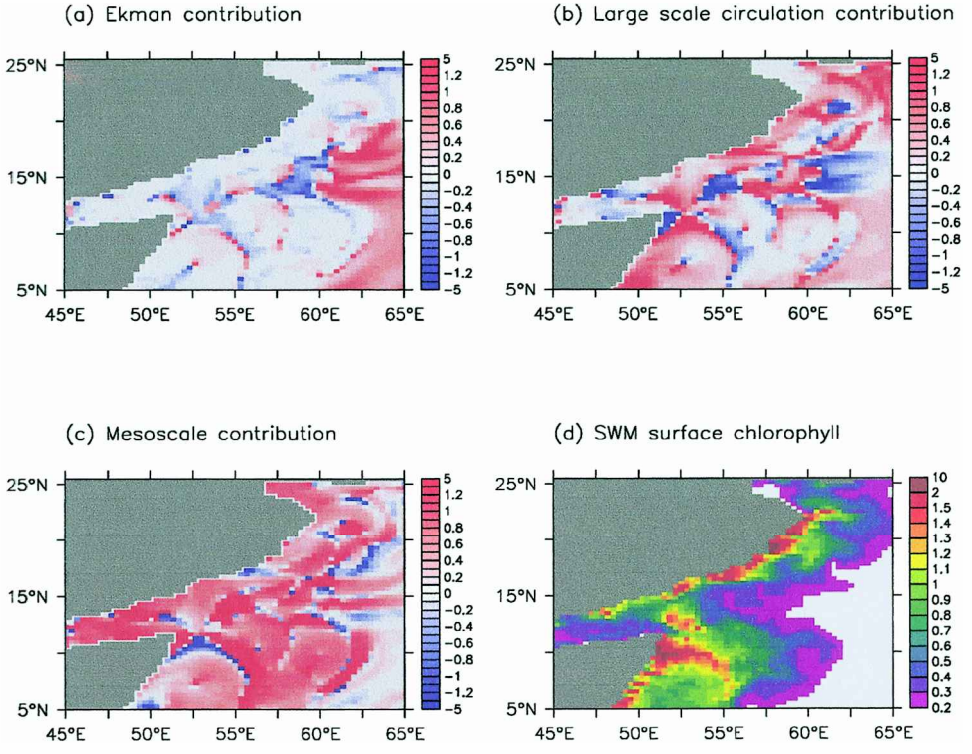

Figure 7. Contribution factor of (a) Ekman transport, (b) large-scale circulation, (c) mesoscale currents to the total horizontal flux of nitrate. See text for the definition of the processes and the contribution factor. The simulated surface chlorophyll concentration in μg/l, averaged over the upper 20 m and June–September, is displayed in (d) for comparison.

The mean flux of horizontal nitrate transport over the upper 60 m during the SWM season can be obtained as

$$\mathbf{F}_i = \frac{1}{121 \text{ days}} \frac{1}{60 \text{ m}} \int_{\text{Jun. 1}}^{\text{Sep. 30}} \int_{60 \text{ m}}^{0 \text{ m}} N\mathbf{u}_i dz dt, \tag{10}$$

where the subscript i is one of ek, lsc, msc and tot, and $\mathbf{F}_i$ is horizontal nitrate flux due to the process i. Plotting the vector field of $\mathbf{F}_i$ should provide a plain view of the mean path of nitrate transport.

b. Contribution from each process

Figure 6 shows the mean path of the nitrate transport decomposed into the three processes (a–c) and the total transport (d). In the total transport field, the effect of the Great

(a)

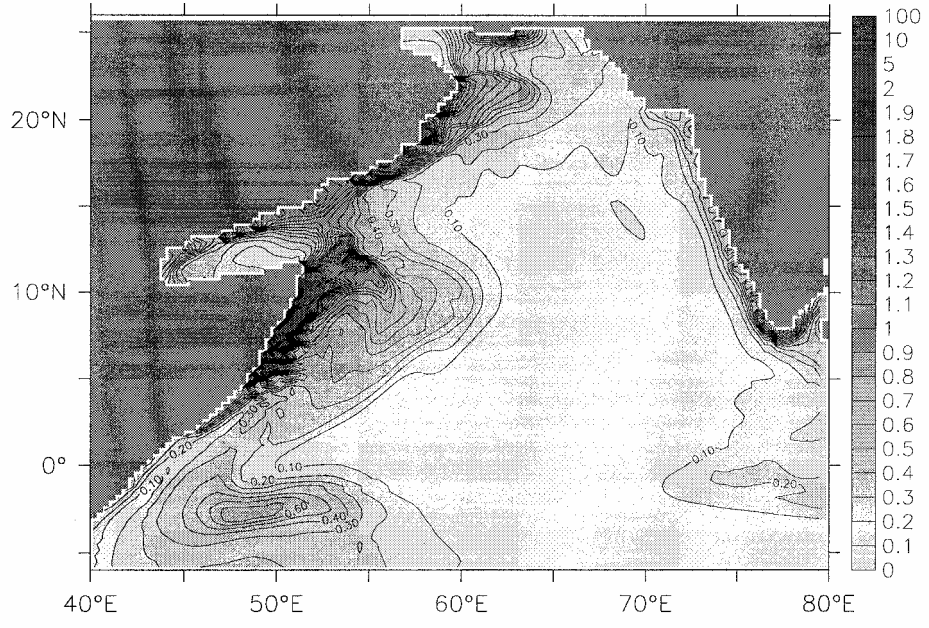

Figure 8. (a) Chlorophyll distribution averaged over the upper 20 m and June–September, in an experiment where horizontal viscosity is enhanced (viscous run) so that it emulates a coarse resolution model. Units are μg/l.

Whirl and the Socotra Gyre is clearly visible. A path from the Great Whirl to the southern fraction of the coast of Oman indeed exists, as has been shown in Figure 5a. In the north, northeastward transport along the coast can be found while there is a vortex structure slightly offshore.

A question addressed naturally is which process is contributing most to form the total transport field. Apparently, the mesoscale transport field bears the highest resemblance to the total transport field. To visualize the resemblance more clearly, we devise a quantity c_i, which will be called the contribution factor, as a measure of significance of the process i to the total transport:

$$c_i = \frac{\mathbf{F}_i \cdot \mathbf{F}_{\text{tot}}}{|\mathbf{F}_{\text{tot}}|^2}, \tag{11}$$

that is, the component of $\mathbf{F}_i$ in the direction of $\mathbf{F}_{\text{tot}}$ normalized by the length of $\mathbf{F}_{\text{tot}}$. For example, when $\mathbf{F}_i$ is exactly the same as $\mathbf{F}_{\text{tot}}$, c_i becomes one, and when $\mathbf{F}_i$ is toward the direction opposite to that of $\mathbf{F}_{\text{tot}}$, c_i becomes negative.

The contribution factors are shown in Figures 7a–c. Simulated surface chlorophyll

(b)

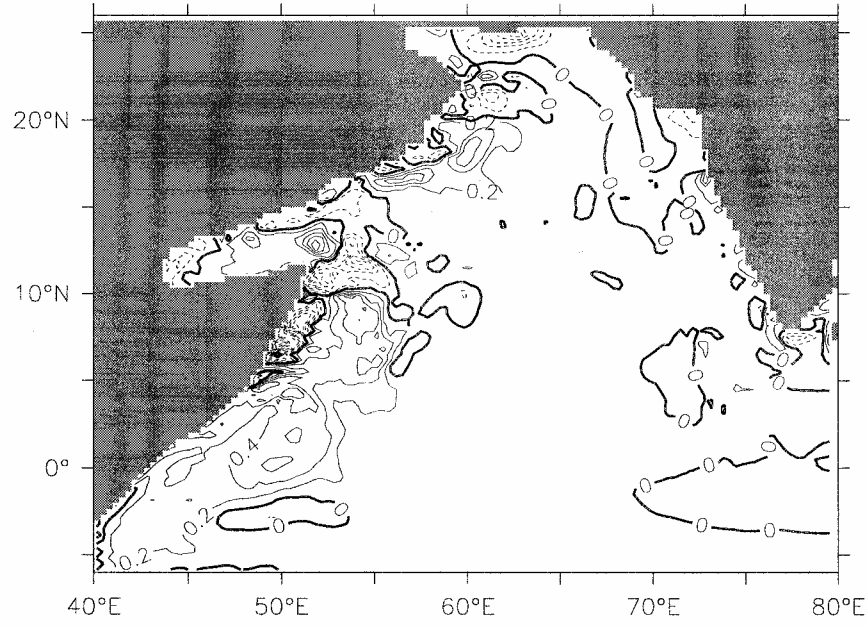

Figure 8. (Continued) (b) Difference in surface chlorophyll during the SWM season between the standard run and the viscous run. That is, the difference between Figure 2a and the upper panel. Positive values mean that chlorophyll is more abundant in the standard run. Contour intervals are 0.2 μg/l.

concentration averaged over the SWM season is displayed in Figure 7d to facilitate comparison. As could be expected from Figure 6, the contribution from the mesoscale transport dominates the field, followed by that from the large-scale circulation. It is seen that the large-scale circulation is playing the major role in carrying nitrate along the coasts of Somalia and Oman, and the northern periphery of the Great Whirl. For the other regions where the surface chlorophyll increases during the SWM season, the mesoscale transport is the main factor for the horizontal nitrate flux. The contribution of the Ekman transport is, on the other hand, extremely small being somewhat contrary to a common notion (Bartolacci and Luther, 1999). Comparison between Figures 7a and d reveals that the Ekman transport is of importance only in the region in which the phytoplankton growth is not stimulated during the SWM season.

c. Biology in the viscous run

The importance of mesoscale currents also can be evidenced by comparing the surface chlorophyll concentrations in the standard and the viscous run. Surface

chlorophyll in the third year of the viscous run averaged over the SWM season (Fig. 8a) is subtracted from that of the standard run (Fig. 2a), and the result is given in Figure 8b; here, positive values mean that surface chlorophyll is more abundant in the standard run.

Within the Great Whirl and off the coast of Oman, chlorophyll is increased significantly in the standard run being consistent with the analysis made so far. In the northern end, however, chlorophyll is decreased in the standard run. This is because less nitrate can be advected along the coast of Oman to the northeast in the standard run due to disposal of nitrate to the offshore direction by mesoscale transport. Furthermore, on the northeast of the Great Whirl, chlorophyll is not so much increased as would be expected from Figure 7c. This is again partly due to the nitrate disposal in the standard run by mesoscale transport into the Great Whirl during the nitrate transport along the coast of Somalia. Another factor is that the Great Whirl is shifted northward in the viscous run, thereby carrying nitrate into the region where mesoscale transport would be dominant in the standard run. The absolute values in Figure 8b amount to ~30–100% of those in Figure 2a, thereby confirming the importance of mesoscale transport.

d. Sensitivity to wind forcing

The results obtained so far are basically the same for other years of coupled integration (figures not shown). A sensitivity experiment on wind forcing is further performed by using the one by daSilva *et al.* (1994) based on the Comprehensive Ocean-Atmosphere Data Set (COADS), instead of that by Barnier *et al.* (1995) adopted in the standard and viscous run. The distribution of the contribution factor in this experiment (Fig. 9) is not very much modified compared with that in the control case (Fig. 7): the Ekman transport is of minimal importance in the high chlorophyll band; the contributions from mesoscale currents and large-scale circulation are collaborating to transport nutrient, though the latter accounts more than it does in the control case. Thus the contribution assignment between the mesoscale currents and the large-scale circulation may depend on the wind forcing used, but it would always be true that little can be ascribed to the Ekman transport.

e. Discussion

One may criticize the way we separated the large-scale circulation and the mesoscale currents because the large-scale circulation itself often changes when mesoscale currents are introduced in a numerical model. However, such an effect can be large mainly when the current is so strong that the nonlinear terms become important. In the present study it occurs only around the Great Whirl, and otherwise the present method works well. Our focus is on nitrate transport to outside the Great Whirl and to the offshore regions from the coasts of Somalia and Oman. Therefore, we do not consider that our argument is severely spoiled by this criticism, though we do not intend to put too much emphasis on the contribution assignment between the large-scale circulation and the mesoscale currents; at

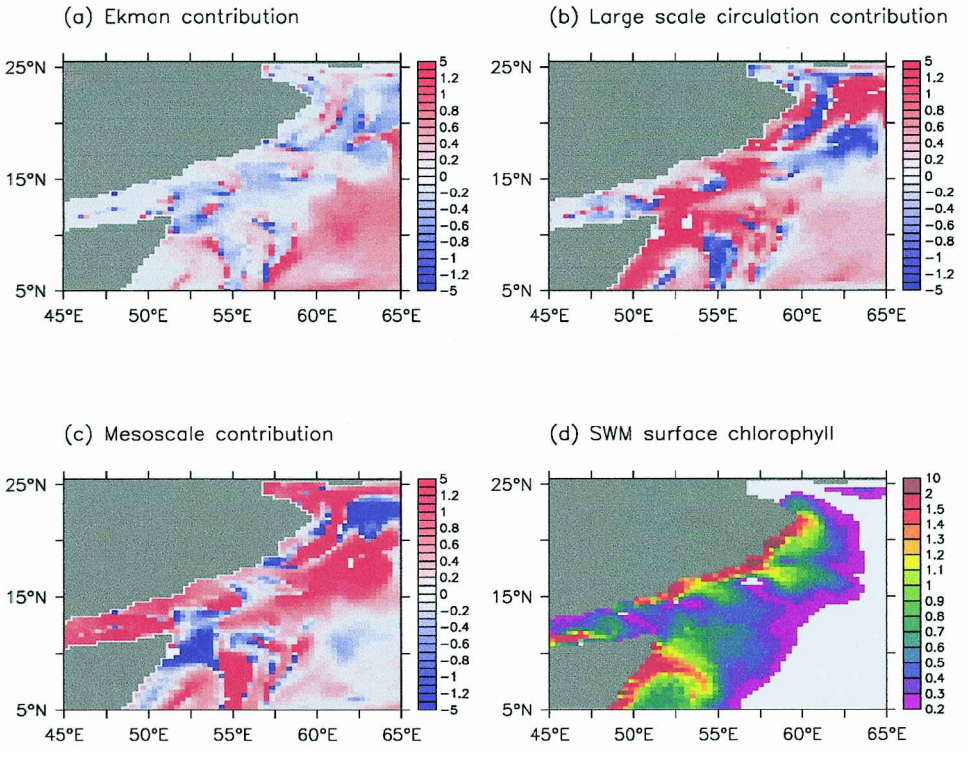

Figure 9. Contribution factor. As in Figure 7 but for an experiment with a different wind stress dataset (daSilva *et al.,* 1994).

least the statement that the Ekman transport is not the main agent of nutrient transport is not affected.

Another point that should be mentioned is that the Ekman transport is not negligible when one looks at the horizontal advection term in the governing equation of nitrate (i.e., $\mathbf{u}_i \cdot \nabla_h N$), instead of horizontal transport (i.e., $\mathbf{u}_i N$). Figure 10 shows the term integrated over the SWM season and averaged over the upper 60 m. It is seen that the contribution from the Ekman transport is in fact significant compared with that from the other two, while the Ekman transport is not participating in the horizontal nitrate transport (Figs. 6 and 7). This apparently puzzling situation takes place because the Ekman transport is often directed across the isolines of nitrate concentration, while the flows due to the other two are often along the isolines. Namely, this results from the very fact that the Ekman transport is not transporting nitrate. The Ekman transport can be significantly contributing in the horizontal advection term, but it is a passive contribution in that it relies on the transport by other processes. In other words, the main role of the Ekman transport is to deposit nitrate that has been carried to a certain location by the large-scale circulation or the mesoscale currents, or both.

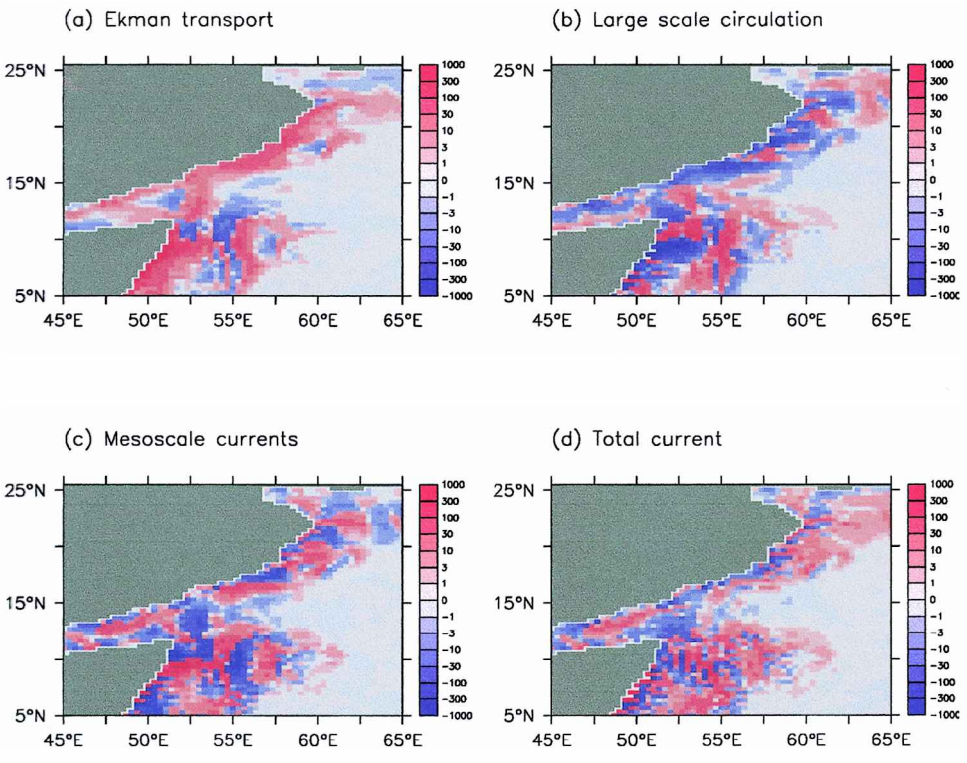

Figure 10. Horizontal advection term ($\mathbf{u}_i \cdot \nabla_h N$) averaged over the upper 60 m and integrated over June–September due to (a) Ekman transport, (b) large-scale circulation, (c) mesoscale currents and (d) total current. Units are mmol/m^3.

Finally, it is noteworthy that some of the mesoscale features in the model stay unmoved for longer time periods (several months or more) than those often associated with mesoscale phenomena. This is why the mesoscale features are so evident in Figures 6c,d even in a four-month mean field, which is relatively a long time scale for mesoscale phenomena. Moreover, they tend to appear at approximately the same locations every year. The prominent vortex structures in Figure 6c centered at 10N, 57E (Socotra Gyre), 18N, 59E, and 22N, 61E are formed in other years of coupled integration as well. These repeated, long-lived structures are playing an important role in nutrient transport.

5. On the model's underestimate of surface chlorophyll

It has been demonstrated that mesoscale currents are responsible for the high chlorophyll during the SWM season off the coasts of Oman and Somalia. A close look at Figure 2 can, however, reveal that to the north of ~12N, the band of high chlorophyll does not extend enough to the southeast. Also, Kawamiya and Oschlies (2001) pointed out that the nitrate

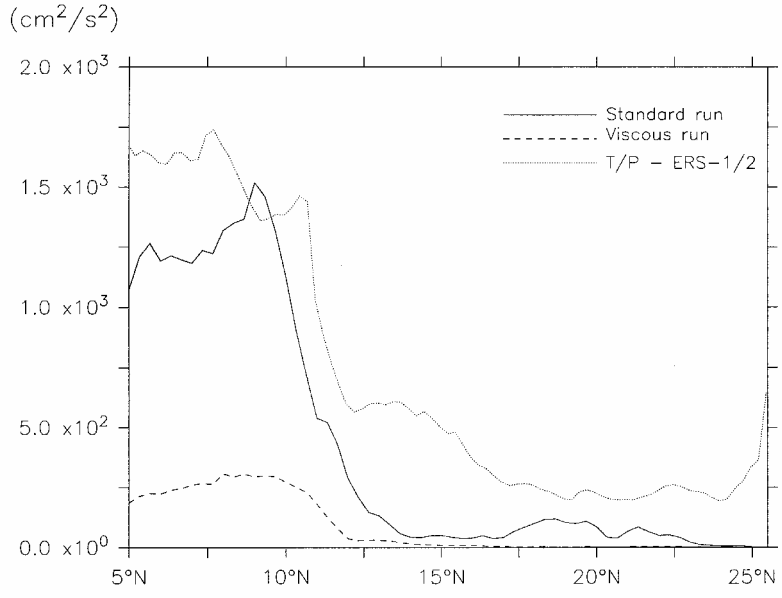

Figure 11. Surface eddy kinetic energy (EKE) averaged over June–September and 45E–65E, from model runs and satellite-based estimate using TOPEX/Poseidon-ERS-1/2 data. See text for the definition of EKE for the model results. Satellite-based estimate is a 5-year mean from 1995 to 1999. The altimeter products were produced by the CLS Space Oceanography Division as part of the Environment and Climate EU AGORA (ENV4-CT9560113) and DUACS (ENV44-T96-0357) (Le Traon and Ogor, 1998; Le Traon *et al.,* 1998).

supply in the model during the SWM season is not enough at S04, a U.S.JGOFS station located off the coast of Oman (17N, 60E).

From the argument in the previous sections, it is inferred that mesoscale currents may not be active enough in the model. To check whether or not they are active enough, we adopt the surface eddy kinetic energy (EKE) as a measure of mesoscale activity. EKE in the standard run is defined as $1/2\mathbf{u}' \cdot \mathbf{u}'$ where $\mathbf{u}'$ is horizontal velocity deviation from a 3-year (from the fourth to the sixth year) mean field of coupled integration. EKE is calculated at the depth of 65 m to exclude Ekman currents and displayed in Figure 11 with satellite-based data after averaging over the SWM season and for the range 45E–65E (i.e., the longitudinal range of Figure 6 and Figure 7). EKE in the viscous run is also exhibited here so that one can see that eddies are indeed activated in the standard run.

One should note, however, that EKE defined here is different from the energy contained in the field of mesoscale currents. The energy of mesoscale currents would be larger than EKE in the model because the simulated mesoscale currents tend to form in a similar place every year. Unfortunately, there is no observational estimates corresponding to the mesoscale currents we defined. The EKE field is the closest observational product to the energy of mesoscale field.

EKE in the standard run agrees well with the data to the south of ~12N, but to the north of it, the model always underestimates EKE at least by a factor of 2 and sometimes even by an order of magnitude. One may recall that the modeled high chlorophyll band is narrower than observed indeed to the north of ~12N (Fig. 2). It is probable that this underestimate of EKE is the cause for the insufficiency of the spatial extent of the band. Even more active eddy formation may have to be simulated to obtain a more realistic chlorophyll enhancement during the SWM season, using a finer resolution model or an assimilation method by, e.g., Oschlies and Willebrand (1996). Note, however, that the mechanism for chlorophyll enhancement by mesoscale currents enlightened in this study is different from that suggested by Woods (1988), McGillicuddy and Robinson (1997) and McGillicuddy *et al.* (1998). They emphasized vertical pumping of nutrient by mesoscale eddies, while this study focuses on the horizontal transport. On the other hand, Garçon *et al.* (2001) pointed out that horizontal nutrient transport by mesoscale currents was also the major cause for the increase in biological production in the subtropical gyre of the North Atlantic model by Oschlies and Garçon (1998).

6. Summary and conclusion

The mechanism of the surface phytoplankton bloom in the western Arabian Sea during the SWM season has been investigated using a biological-physical coupled model with an eddy-permitting resolution. With the "labeled nitrate," which can track the fate of nitrate through both biological and physical transport, it was shown that the open ocean upwelling is not a major factor and that horizontal nitrate transport subsequent to the coastal upwelling is the key.

There are three possible carriers for the horizontal transport, the Ekman transport, the transport by the large-scale circulation and that by mesoscale currents. Relative importance of the three was estimated by quantifying the similarity between the horizontal nitrate flux field by the total transport and that by each process. The result from the control case is that the mesoscale transport accounts for most of the total transport, followed by the large-scale transport, though this ranking depends on the wind forcing. The Ekman transport is not participating in carrying nitrate within the high-chlorophyll band. Though it can be significant in the horizontal advection term, it is only in a subordinate sense.

Comparison of EKE between the model and satellite observations showed that the eddy activity in the model is not vigorous enough especially to the north of ~12N. This may explain the simulated extent of the high-chlorophyll band narrower than in the satellite data. Adopting a higher resolution or assimilating sea-surface-height data may be necessary for reproducing a wider band of high chlorophyll during the SWM season.

Acknowledgments. This study is a contribution to the German JGOFS program. I am very much obliged to Andreas Oschlies for reading the draft carefully and for many helpful discussions. The comments from Achim Wirth were also helpful. I thank Thomas Martin for processing SeaWiFS data. Comments from Robert Weller and the anonymous reviewer improved the manuscript. The software, FERRET, was extensively used for the analysis and graphics.

REFERENCES

Banse, K. 1987. Seasonality of phytoplankton chlorophyll in the central and northern Arabian Sea. Deep-Sea Res., *34,* 713–723.

Barnier, B., L. Siefridt and P. Marchesiello. 1995. Surface thermal boundary condition for a global ocean circulation model from a three-year climatology of ECMWF analysis. J. Mar. Syst., *6,* 363–380.

Bartolacci, D. M. and M. E. Luther. 1999. Patterns of co-variability between physical and biological parameters in the Arabian Sea. Deep-Sea Res. II., *46,* 1933–1964.

Conkright, M. E., S. Levitus and T. P. Boyer. 1994a. World Ocean Atlas 1994, Vol. 1 NOAA Atlas NESDIS, NODC.

——1994b. World Ocean Atlas 1994, Vol. 1, nutrients, NOAA Atlas NESDIS 1: Technical report, NODC.

Cushman-Roisin, Benoit. 1994. Introduction to Geophysical Fluid Dynamics, Prentice Hall, NJ, 320 pp.

daSilva, A. M., C. C. Young and S. Levitus. 1994. Atlas of Surface Marine Data, NOAA. Atlas NESDIS, US Department of Commerce, Washington, DC.

Dickey, T., J. Marra, D. E. Sigurdson, R. A. Weller, C. S. Kinkade, S. E. Zedler, J. D. Wiggert and C. Langdon. 1998. Seasonal variability of bio-optical and physical properties in the Arabian Sea: October 1994–October 1995. Deep-Sea Res. II., *45,* 2001–2025.

Fasham, M. J. R., H. W. Ducklow and S. M. McKelvie. 1990. A nitrogen based model of plankton dynamics in the oceanic mixed layer. J. Mar. Res., *48,* 591–639.

Fischer, A. S., R. A. Weller, D. L. Rudnick, C. C. Eriksen, C. M. Lee, K. H. Brink, C. A. Fox and R. R. Leben. 2001. Mesoscale eddies, coastal upwelling, and the upper ocean heat budget in the Arabian Sea. Deep-Sea Res. (submitted).

Flagg, C. N. and H.-S. Kim. 1998. Upper ocean currents in the northern Arabian Sea from shipboard ADCP measurements collected during the 1994–1996 U.S.JGOFS and ONR programs. Deep-Sea Res. II., *45,* 1917–1959.

Garçon, V. C., A. Oschlies, S. C. Doney, D. McGillicuddy and J. Waniek. 2001. The role of mesoscale variability on plankton dynamics in the North Atlantic. Deep-Sea Res. II., *48,* 2199–2226.

Haney, R. L. 1971. Surface thermal boundary condition for ocean circulation models. J. Phys. Oceanogr., *1,* 241–248.

Kawamiya, M. and A. Oschlies. 2001. An eddy-permitting, coupled ecosystem-circulation model of the Arabian Sea: Comparison with observations. J. Mar. Syst., (submitted).

Keen, T. R., J. C. Kindle and D. Young. 1997. The interaction of southwest monsoon upwelling, advection and primary production in the northwest Arabian Sea. J. Mar. Syst., *13,* 61–82.

Le Traon, P.-Y., F. Nadal and N. Ducet. 1998. An improved mapping method of multi-satellite altimeter data. J. Atmos. Ocean. Technol., *15,* 522–534.

Le Traon, P.-Y. and F. Ogor. 1998. ERS-1/2 orbit error improvement using TOPEX/Poseidon: the 2 cm challenge. J. Geophys. Res., *103,* 8045–8057.

Levitus, S. and T. P. Boyer. 1994a. World Ocean Atlas 1994, Vol. 3, salinity, NOAA Atlas NESDIS 3 Technical report, NODC.

——1994b. World Ocean Atlas 1994, Vol. 4, temperature, NOAA Atlas NESDIS 4 Technical report, NODC.

Madhupratap, M. and A. H. Parulekar. 1993. Biological processes of the northern Indian Ocean, *in* Monsoon Biogeochemistry, SCOPE/UNEP, *76,* Geologisch-Paläontologischen Institut der Universität Hamburg, 51–72.

Manghnani, V., J. M. Morrison, T. S. Hopkins and E. Böhn. 1998. Advection of upwelled waters in the form of plumes off Oman during the Southwest Monsoon. Deep-Sea Res. II., *45,* 2027–2052.

McGillicuddy, D. J. and A. R. Robinson. 1997. Eddy-induced nutrient supply and new production in the Sargasso Sea. Deep-Sea Res., *44,* 1427–1450.

McGillicuddy, D. J., A. R. Robinson, D. A. Siegel, H. W. Jannasch, R. Johnson, T. D. Dickey, J. McNeil, A. F. Michaels and A. H. Knap. 1998. Influence of mesoscale eddies on new production in the Sargasso Sea. Nature, *394,* 263–266.

Morrison, J. M., L. A. Codispoti, S. Gaurin, B. Jones, V. Manghnani and Z. Zheng. 1998. Seasonal variation of hydrographic and nutrient fields during the US JGOFS Arabian Sea Process Study. Deep-Sea Res. II., *45,* 2053–2101.

Numaguti, A. 1999. Origin and recycling processes of precipitating water over the Eurasian continent: Experiments using an atmospheric general circulation model. J. Geophys. Res., *104,* 1957–1972.

Oschlies, A. and V. Garçon. 1998. Eddy-induced enhancement of primary production in a model of the North Atlantic Ocean. Nature, *394,* 266–269.

——1999. An eddy-permitting coupled physical-biological model of the North Atlantic 1. Sensitivity to advection numerics and mixed layer physics. Glob. Biogeochem. Cycles, *13,* 135–160.

Oschlies, A. and J. Willebrand. 1996. Assimilation of Geosat altimeter data in an eddy-resolving primitive equation model of the North Atlantic Ocean. J. Geophys. Res., *101,* 14175–14190.

Pacanowski, R. C. 1995. MOM 2 documentation, user's guide and reference manual, Technical Report 3, GFDL Ocean.

Pacanowski, R. C. and S. G. H. Philander. 1981. Parameterization of vertical mixing in numerical models of tropical oceans. J. Phys. Oceanogr., *11,* 1443–1451.

Rix, N. H. 1998. Investigating Indian Ocean Variability in a Basin Scale GCM: Model Assessment and Model-Data Intercomparison. PhD thesis, Universität Kiel, 155 pp.

Rixen, T., B. Haake, V. Ittekkot, M. V. S. Guptha, R. R. Nair and P. Schlüssel. 1996. Coupling between SW monsoon-related surface and deep ocean processes as discerned from continuous particle flux measurements and correlated satellite data. J. Geophys. Res., *101,* 28,569–28,582.

Stephens, D. P. 1991. The open boundary condition in the United Kingdom Fine-Resolution Antarctic Model. J. Phys. Oceanogr., *21,* 1494–1499.

Woods, J. D. 1988. Mesoscale upwelling and primary production, *in* Toward a Theory on Biological-Physical Interactions in the World Ocean, B. J. Rothschild, ed., Kluwer Academic Publishers, Dordrecht, 7–38.

Young, D. K. and J. C. Kindle. 1994. Physical processes affecting availability of dissolved silicate for diatom production in the Arabian Sea. J. Geophys. Res., *99,* 22619–22632.

Received: *8 February, 2001;* revised: *22 June, 2001.*